

The no-hair theorems at work in the tidal disruption event AT2020afhd

Lorenzo Iorio 

Ministero dell' Istruzione e del Merito
Viale Unità di Italia 68, I-70125, Bari, Italy
email: lorenzo.iorio@libero.it

February 25, 2026

Abstract

Recently, the coprecession of both the accretion disk and the jet formed following the tidal disruption event associated with the optical transient AT2020afhd, driven by a supermassive black hole of almost ten million solar masses, were independently measured in both the X and radio bands, respectively, showing a periodicity of nearly 20 days over about 300 days. An analytical model of the general relativistic gravitomagnetic Lense-Thirring precession of the effective orbit of a fictitious test particle revolving about a spinning primary can explain the observed precessional features. It yields allowed regions in the system's parameter space which, as far as the hole's dimensionless spin parameter is concerned, are essentially in agreement with those obtained in the literature with general relativistic magnetohydrodynamic simulations. The present analytical approach can be extended to include the precession due to the hole's quadrupole mass moment as well. It breaks the degeneracy in the allowed regions occurring for negative and positive values of the spin parameter when only the Lense-Thirring effect is considered. The best estimate for the hole's mass yields the range 0.185 – 0.215 for the dimensionless spin parameter. Using the same strategy with the gravitomagnetic frequency for an extended disk of finite size with a parameterized power-law mass density yields to distinct, generally non-overlapping allowed regions for each value of the power-law index adopted.

keywords— Classical black holes; General relativity; Accretion disk & black-hole plasma; Astronomical black holes

1 Introduction

Tidal disruption events (TDEs), first theoretically predicted by Hills (1975), occur when main sequence stars, passing by a supermassive black hole (SMBH), or, more compactly, megapyknon (MP) (Iorio, 2025c), like those that lurk in the core of several galaxies, are torn apart by the tidal forces due to the intense gradient of the gravitational field of the latter (Rees, 1988; Evans and Kochanek, 1989; Mockler et al., 2026). The resulting debris arranges itself in orbit around the black hole (BH), forming temporarily a rapidly circularized (Hayasaki et al., 2016) thick accretion disk (Ulmer, 1999; Strubbe and Quataert, 2009) around the tidal radius initially inclined with respect to the hole's equatorial plane (Canizzo et al., 1990). Over time, it tends to align with the latter's spin due to concomitant magnetic forces acting on the ionized particles of the disk itself (McKinney et al., 2013). The resulting complex physical environment around the accreting BH (Dai et al., 2021) can also sometimes induce the formation

of a moderately relativistic jet (De Colle and Lu, 2020; Foschini, 2022; Foschini et al., 2024) that, for periods ranging from a few months to a few years, is often visible by emitting electromagnetic waves in the radio band, while the accreting matter pour outs X-rays. As long as the disk’s misalignment with respect to the equator persists, complex general relativistic magnetohydrodynamic (GRMHD) simulations predict that the jet and the disk remain tightly coupled (Liska et al., 2018; Chatterjee et al., 2020), exhibiting a coprecessional motion that is commonly attributed to the general relativistic gravitomagnetic Lense-Thirring (LT) effect (Fragile et al., 2007; Stone and Loeb, 2012; Franchini et al., 2016; Pasham et al., 2024). At this point, it may be useful to clarify that denominations like ‘gravitomagnetism’ have nothing to do with any interplay between gravitation and genuine magnetic forces, being just due to the formal resemblance of the linearized Einstein field equations of general relativity in the weak-field and slow-motion limit with the linear Maxwell’s ones for electromagnetism (Thorne et al., 1986; Thorne, 1986, 1988; Jantzen et al., 1992; Mashhoon, 2001; Ruggiero and Tartaglia, 2002; Mashhoon, 2007). Within such an approximation, the off-diagonal terms of the spacetime metric tensor give rise to an acceleration felt by a test particle orbiting a massive rotating body which looks like that due to the Lorentz force experienced by an electric charge moving in a magnetic field. Within the context of TDEs, the LT effect leaves a characteristic signature in both the X-ray and radio emission in the form of quasi-periodic modulations that, up to now, have never been observed simultaneously, having instead been measured either in X-rays (Saxton et al., 2012; Ma et al., 2021; Pasham et al., 2024) or in the radio band (Cui et al., 2023; Tian et al., 2023) separately.

This situation has recently changed with the TDE associated with the substantial rebrightening¹ in 2024 of the optical transient AT2020afhd/ZTF20abwtifz that occurred in 2020 in the galaxy LEDA 145386 where both X-ray and radio signals from the disk-jet coprecession were simultaneously measured for the first time (Wang et al., 2025). The resulting picture, emerging from a data analysis spanning about 300 days, encompasses a Kerr SMBH of about ten million solar masses which, rotating rather slowly dragged a mildly misaligned disk into a precession with a period of about 20 days; see Table 1 for the relevant parameters of this TDE.

Table 1: Physical and orbital parameters of the TDE associated with AT2020afhd as determined by Wang et al. (2025). The mass of the SMBH is M_{\bullet} , while the Sun’s mass is denoted by M_{\odot} . The period of the disk-jet coprecession, in days, is T_{prec} . The angle θ_i is counted from the reference z axis of the coordinate system adopted in Fig. 5 (A) of Wang et al. (2025), whose direction is assumed equal to that of the SMBH’s symmetry axis, to the unit vector \hat{h} of the disk’s orbital angular momentum, while $\phi_{\text{obs}}, \theta_{\text{obs}}$ are the longitude and colatitude, respectively, of the line of sight.

$\log(M_{\bullet}/M_{\odot})$	$T_{\text{prec}} \text{ (d)}$	$\theta_i \text{ (}^{\circ}\text{)}$	$\phi_{\text{obs}} \text{ (}^{\circ}\text{)}$	$\theta_{\text{obs}} \text{ (}^{\circ}\text{)}$
6.7 ± 0.5	19.6 ± 1.5	14.5 ± 0.5	188.4 ± 1.5	$38.4^{+0.5}_{-0.6}$

In this paper, it is shown that it is possible to obtain the same results about the LT hypothesis and the SMBH’s spin with a very simple analytical model, formally accurate to the first post Newtonian (1pN) level, of the gravitomagnetic precession of the orbital angular momentum of a fictitious test particle moving along a sort of ‘effective’ circular orbit (Barker and Oconnell, 1974; Iorio, 2025b) whose radius equals the tidal disruption one for the SMBH considered. Such a picture could even be something more than a simple effective phenomenological artifice since GRMHD simulations show that the disks expected in TDEs do, indeed, rotate rigidly (Fragile et al., 2007; Dexter and Fragile, 2011). It can be further enriched by quantifying also the contribution of the SMBH’s quadrupole mass moment (Iorio, 2025a) in the present case, neglected by Wang et al. (2025). The same approach, which can be

¹Its observed optical decay rate is in agreement with the debris fallback rate expected in TDE theories.

straightforwardly extended to other systems like the one considered here, was successfully adopted in [Iorio \(2025a,b\)](#) also for the recently measured jet precession emanating from the surrounding of the SMBH M87* ([Cui et al., 2023](#); [Cui and Lin, 2025](#)). It may be viewed as another unexpected example of the ‘the unreasonable effectiveness of the post-Newtonian approximation in gravitational physics’ ([Will, 2011](#)).

The paper is organized as follows. The mathematical model assumed for effectively describing the disk-jet coprecession is described in Section 2. It is applied to infer constraints on the system’s parameters in Section 3. Section 4 is devoted to an analysis of the bounds obtained by [Wang et al. \(2025\)](#) with a disk of finite size endowed with a power-law density profile. Section 5 summarizes the present findings and offers conclusions.

2 The mathematical model of the no-hair disk precession

The precession of the unit vector $\hat{\mathbf{h}}$ of the orbital angular momentum of a test particle orbiting a massive object of mass M , angular momentum J and dimensional quadrupole mass moment Q_2 , with $[Q_2] = \text{ML}^2$, is

$$\frac{d\hat{\mathbf{h}}}{dt} = \boldsymbol{\Omega} \times \hat{\mathbf{h}}, \quad (1)$$

In it, the angular velocity vector $\boldsymbol{\Omega}$ of the precession is

$$\boldsymbol{\Omega} = \Omega \hat{\mathbf{k}}, \quad (2)$$

where $\hat{\mathbf{k}}$ is the primary’s spin axis, and ([Iorio, 2025a,b](#))

$$\boldsymbol{\Omega} = \Omega_{\text{LT}} + \Omega_{Q_2} = \frac{2GJ}{c^2 p^3 (1 - e^2)^{-3/2}} + \frac{3n_{\text{K}} Q_2}{2Mp^2} \hat{\mathbf{k}} \cdot \hat{\mathbf{h}}. \quad (3)$$

In Equation (3), G is the Newtonian constant of gravitation, c is the speed of light in vacuum, e is the orbital eccentricity, p is the orbital semilatus rectum which, in the limit $e \rightarrow 0$, reduces to the orbital radius r_0 , and

$$n_{\text{K}} := \sqrt{\frac{GM(1 - e^2)^3}{p^3}} \quad (4)$$

is the Keplerian mean motion which can be rewritten as

$$n_{\text{K}} = \sqrt{\frac{GM}{r_0^3}} \quad (5)$$

for a circular orbit.

In the case of the Kerr metric ([Kerr, 1963, 1965](#); [Visser, 2009](#); [Teukolsky, 2015](#)), which is believed to describe the exterior spacetime of a spinning BH ([Bardeen, 1970](#)), the so-called ‘no-hair’ (NH) theorems ([Israel, 1967](#); [Carter, 1971](#); [Robinson, 1975](#)), as per the fortunate aphorism by J.A. Wheeler ([Ruffini and Wheeler, 2009](#)), predict that, contrary to an ordinary nonspherical material body, all the mass and spin multipole moments \mathcal{M}_\bullet^ℓ and \mathcal{J}_\bullet^ℓ of degree $\ell = 0, 1, 2, \dots$, respectively, can be expressed as² ([Geroch, 1970](#); [Hansen, 1974](#); [Thorne, 1980](#))

$$\mathcal{M}_\bullet^\ell + i\mathcal{J}_\bullet^\ell = M_\bullet \left(i \frac{J_\bullet}{cM_\bullet} \right)^\ell, \quad (6)$$

²The formalisms by Geroch-Hansen and Thorne were proven to be equivalent, up to a normalization factor, by [Gürsel \(1983\)](#).

where $i := \sqrt{-1}$ is the imaginary unit. From Equation (6), it turns out that the odd mass moments and the even spin moments vanish; the mass moment of degree $\ell = 0$ is nothing but the BH's mass, while the spin moment of degree $\ell = 1$ is proportional to its spin angular momentum. For a Kerr BH, the latter is (Shapiro and Teukolsky, 1986)

$$J_{\bullet} = a_{\bullet} \frac{M_{\bullet}^2 G}{c}; \quad (7)$$

Equation (7) comes from the condition that the g_{rr} component of the Kerr metric in the Boyer-Lindquist coordinates (Boyer and Lindquist, 1967) goes to infinity. The quadrupole mass moment, namely the mass moment M_{\bullet}^2 of degree $\ell = 2$ in Equation (6) renamed here as Q_2^{\bullet} , is

$$Q_2^{\bullet} = -\frac{J_{\bullet}^2}{c^2 M_{\bullet}}. \quad (8)$$

In Equation (7), a_{\bullet} is the dimensionless spin parameter (Bardeen et al., 1972) which can be viewed as the second characteristic length³

$$l_g := \frac{J_{\bullet}}{c M_{\bullet}} \quad (9)$$

entering the Kerr metric measured in units of the BH's gravitational radius

$$R_g := \frac{G M_{\bullet}}{c^2}. \quad (10)$$

The value of a_{\bullet} must fulfil the condition

$$|a_{\bullet}| \leq 1; \quad (11)$$

if

$$|a_{\bullet}| = 1, \quad (12)$$

the Kerr BH is said maximally rotating, or extremal. Despite mathematically possible, the actual physical existence of extremal BHs is debated; see, e.g., Dafermos (2025); Coviello and Gregory (2025), and references therein. Should it be $|a_{\bullet}| > 1$, a naked singularity without a horizon would form (Shapiro and Teukolsky, 1991), that would be prohibited by the still unproven cosmic censorship conjecture (Penrose, 1965, 2002) in the case of the gravitational collapse of a material body; for recent discussions and reviews, see, e.g., (Penrose, 1999; Ong, 2020; Landsman, 2021), and references therein. Remarkably, the absence of a horizon would imply the possibility of causality violations because of closed timelike curves (Calvani et al., 1978; de Felice and Calvani, 1979).

It should be noted that Equation (3) is based on the averaged orbital precessions of the inclination and the longitude of the ascending node of a test particle induced by the Newtonian quadrupole mass moment and the 1pN gravitomagnetic field of a rotating material body (Iorio, 2025a,b). As such, in principle, it is not guaranteed that they also hold if the primary is a Kerr BH. Indeed, to date, no material source for the Kerr metric has yet been found, despite notable efforts (Cohen, 1967; Hernandez, 1967, 1968; Wahlquist, 1968; Israel, 1970; Krasinski, 1978; Haggag and Marek, 1981; Herrera and Jimenez, 1982; Haggag, 1990; Drake and Turolla, 1997; Ali, 2001; Papakostas, 2005; Viaggiu, 2006, 2010; Kyriakopoulos, 2013; Azreg-Aïnou, 2014; Hernandez-Pastora and Herrera, 2017; Chou, 2025). Thus, the latter only describes the exterior spacetime of a spinning BH. Nonetheless, a direct calculation to the order of $\mathcal{O}(1/c^2)$ of

³Dubbed as angular momentum per unit mass or specific angular momentum when geometrized units $G = c = 1$ are adopted, l_g is sometimes denoted in the literature by the same symbol a_{\bullet} which, instead, is used in this paper for its dimensionless counterpart. Caution is in order to avoid confusions with the semimajor axis of a Keplerian orbit, usually denoted as a in celestial mechanics (Murray and Dermott, 1999).

the geodesic equations for a test particle moving in the Kerr metric, expressed in terms of the Kerr-Schild quasi-Cartesian coordinates (Kerr, 1963, 1965), shows that Equation (3) holds also for a Kerr BH, characterized by Equations (7)–(8), provided that the formal replacement

$$J_2 \rightarrow -\frac{Q_2}{MR_c^2} \quad (13)$$

is done. In Equation (13), J_2 and R_c are the dimensionless quadrupole mass moment and equatorial radius, respectively, of the oblate material body acting as primary.

In view of the following developments, it is useful to recall that, for a Kerr BH, the radius of the innermost stable circular orbit (ISCO) (Bardeen et al., 1972)

$$\frac{r_{\text{ISCO}}^+}{R_g} = 3 + Z_2 - \sqrt{(3 - Z_1)(3 + Z_1 + 2Z_2)} \quad (14)$$

in the BH's equatorial plane ranges from $6 R_g$ ($a_\bullet = 0$) to $1 R_g$ ($|a_\bullet| = 1$) if $\hat{\mathbf{k}}_\bullet$ and $\hat{\mathbf{h}}$ are parallel (prograde motion), while its maximum value $9 R_g$ occurs from (Bardeen et al., 1972)

$$\frac{r_{\text{ISCO}}^-}{R_g} = 3 + Z_2 + \sqrt{(3 - Z_1)(3 + Z_1 + 2Z_2)} \quad (15)$$

for $|a_\bullet| = 1$ if $\hat{\mathbf{k}}_\bullet$ and $\hat{\mathbf{h}}$ are antiparallel (retrograde motion). In Equations (14)–(15), it is (Bardeen et al., 1972)

$$Z_1 := 1 + (1 - a_\bullet^2)^{1/3} [(1 + a_\bullet)^{1/3} + (1 - a_\bullet)^{1/3}], \quad (16)$$

$$Z_2 := \sqrt{3a_\bullet^2 + Z_1^2}. \quad (17)$$

If $a_\bullet = 0$, Equations (14)–(17) yield

$$r_{\text{ISCO}}^+ = r_{\text{ISCO}}^- = 6 R_g. \quad (18)$$

Figure 1 shows the plots of r_{ISCO}^\pm as functions of a_\bullet according to Equations (14)–(17). It turns out that

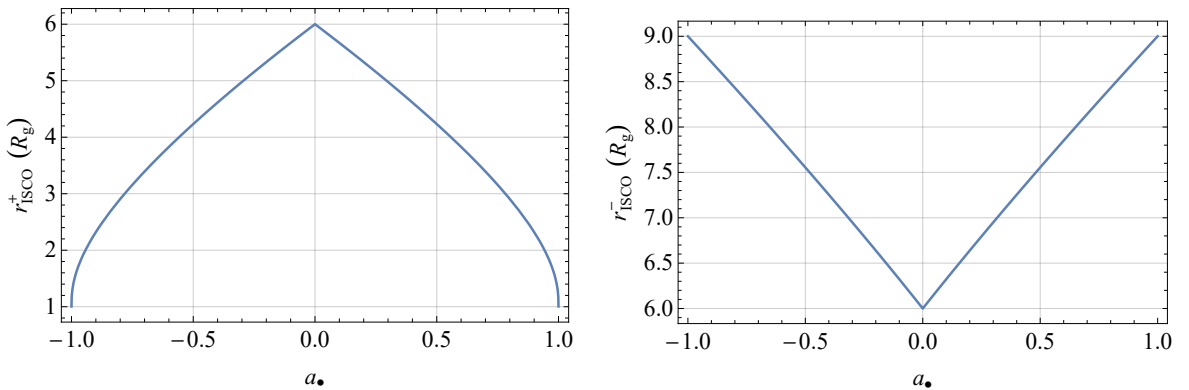


Figure 1: Radii r_{ISCO}^\pm of the prograde (+, left panel) and retrograde (–, right panel) ISCOs, in units of gravitational radii R_g , as functions of the dimensionless spin parameter a_\bullet of a Kerr BH.

the ISCOs' radii are independent of the sign of a_\bullet ; moreover, it is $r_{\text{ISCO}}^- > r_{\text{ISCO}}^+$.

3 Constraining the parameter space

The strategy adopted here consists of identifying the phenomenologically measured precessional frequency of the disk-jet coprecession

$$0.297 \text{ d}^{-1} \leq |\Omega_{\text{obs}}| \leq 0.347 \text{ d}^{-1} \quad (19)$$

with Equation (3). The latter is written with Equations (7)–(8) in order to have the NH precessional angular speed Ω_{NH} for a Kerr BH. Then, it is considered as a function $\Omega_{\text{NH}}(x, y, z, \dots)$ of some system's key physical and orbital parameters as independent variables x, y, z, \dots . Finally, the condition that it must lie within the range of Equation (19) is imposed, namely

$$\Omega_{\text{obs}}^{\text{min}} \leq |\Omega_{\text{NH}}(x, y, z, \dots)| \leq \Omega_{\text{obs}}^{\text{max}} \quad (20)$$

is assumed. In this way, allowed regions in the parameter space $\{x, y, z, \dots\}$ can be obtained.

The reason for which only the absolute value of the precessional frequency or, equivalently, of the precession period T_{prec} can be used resides in the fact that, in such kind of scenarios, one is not allowed to measure the full precession in the three-dimensional space, being only its projection on the plane of the sky accessible to direct observations. This fact can be understood more formally as follows. Let $\hat{\rho}$ the unit vector of the line of sight: its angle with respect to \hat{k}_\bullet is θ_{obs} . Since the SMBH's spin stay fixed, θ_{obs} is constant. The projection of the disk-jet coprecession onto the line of sight is

$$\left| \frac{d\hat{h}}{dt} \right|_\rho := \frac{d\hat{h}}{dt} \cdot \hat{\rho}. \quad (21)$$

According to Equation (1), Equation (21) can be written as

$$\left| \frac{d\hat{h}}{dt} \right|_\rho = \Omega \hat{k}_\bullet \times \hat{h} \cdot \hat{\rho} = \Omega \hat{\rho} \times \hat{k}_\bullet \cdot \hat{h} = \Omega \sin \theta_{\text{obs}} \cos \gamma(t), \quad (22)$$

where $\gamma(t)$ is the time-dependent angle between the constant vector $\hat{\rho} \times \hat{k}_\bullet$, whose modulus is $\sin \theta_{\text{obs}}$, and the precessing unit vector \hat{h} . Since $\sin \theta_{\text{obs}} = \sin(\pi - \theta_{\text{obs}})$, the latter corresponding to $-\hat{k}_\bullet$, Equation (22) cannot discriminate between the two possible senses of the projected precession.

3.1 The parameter space in the most general case

By making the following broad assumptions

1. The cause of the TDE is a SMBH, so that $6 \lesssim \log(M_\bullet/M_\odot) \lesssim 10$ (Furusawa et al., 2023)
2. For tidal disruption to actually occur outside a SMBH, accompanied by detectable flares, it must be $\log(M_\bullet/M_\odot) \lesssim 8$ (Hills, 1975)
3. The external spacetime of the SMBH is described by the Kerr metric
4. The disk likely exhibits a not excessively large tilt to the SMBH's spin axis due to intervening non-gravitational effects of electromagnetic nature, so that $\hat{k}_\bullet \cdot \hat{h} \lesssim 1$
5. The radius of the effective orbit should be at least larger than that of the SMBH's ISCO

the condition of Equation (20) preliminary yields the allowed regions in the three-dimensional parameter space $\{\log(M_\bullet/M_\odot), a_\bullet, r_0\}$ depicted in Figure 2 for both prograde and retrograde ISCOs. About the point 2, it can be explained as follows. If the tidal disruption radius

$$r_t = \left(\frac{M_\bullet}{M_\star}\right)^{1/3} R_\star \quad (23)$$

of a star with mass M_\star and radius R_\star is smaller than the SMBH's event horizon, the star is swallowed whole before being tidally torn apart, and no flares at all are produced. Indeed, a main sequence star moving along an elliptical orbit around a SMBH is dismembered if its pericenter falls within r_t (Rees, 1988; Phinney, 1989; Evans and Kochanek, 1989). The aforementioned condition occurs just for $\log(M_\bullet/M_\odot) \gtrsim 8$ (Hills, 1975). In obtaining them, Equations (14)–(17), valid for equatorial orbits, were

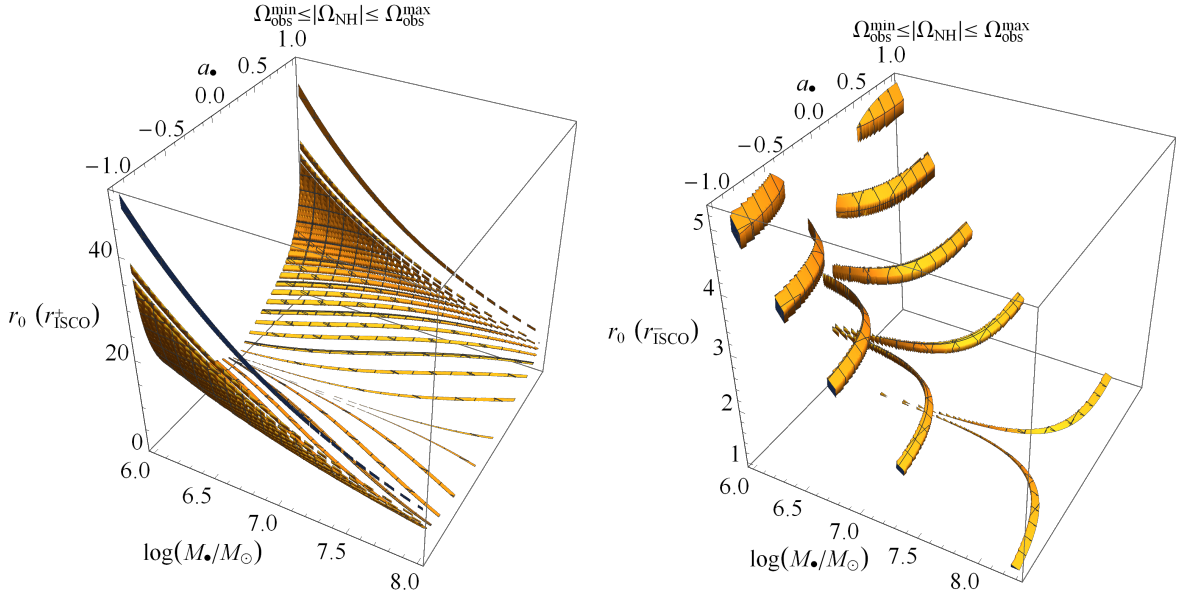


Figure 2: Permitted regions in the three-dimensional parameter space $\{\log(M_\bullet/M_\odot), a_\bullet, r_0\}$ obtained by imposing the conditions that the absolute value of the NH precessional frequency of Equation (3), calculated with Equations (7)–(8), lies within the experimental range of Equation (19) for the observed disk-jet coprecessional one, and that the radius r_0 of the effective test particle orbit is larger than that of the prograde (r_{ISCO}^+ , left panel) and retrograde (r_{ISCO}^- , right panel) equatorial ISCOs. The best estimate of the colatitude θ_i of the orbital angular momentum is taken from Table 1, while $\log(M_\bullet/M_\odot)$ and a_\bullet are allowed to vary within their expected full ranges $6 \lesssim \log(M_\bullet/M_\odot) \lesssim 8$ (Hills, 1975; Furusawa et al., 2023) and $-1 \leq a_\bullet \leq 1$, respectively.

used. Actually, the orbital plane of the effective orbit somehow representative of the precessing disk is not exactly aligned with the hole's equator; thus, strictly speaking, Equations (14)–(17) are not valid. Nonetheless, they could be considered rather good approximations. Indeed, since the orbit's tilt to the hole's equator is assumed to be somewhat small, the left panel of Figure 5 of Kopáček and Karas (2024) shows that, for a turning point's angle, dubbed θ_\star as in Kopáček and Karas (2024), close to 90° , the radii of both the prograde and retrograde innermost stable spherical orbits (ISSOs), extending above and below the BH's equatorial plane for an inclined orbit, essentially agree with those for the ISCOs occurring in the equatorial case. An explanation of the aforementioned angle goes as follows. In standard spherical coordinates, adopted in the Boyer-Lindquist form of the Kerr metric (Boyer and Lindquist, 1967), the coordinate $z_P(t)$ of a point P moving at constant distance r_0 from the center is $z_P(t) = r_0 \cos \theta(t)$,

where $\theta(t)$ is the colatitude angle reckoned from the reference z axis which, in this case, is the SMBH's spin direction. In standard celestial mechanics, it is written as $z_P(t) = r_0 \sin \theta_i \sin u(t)$, where⁴ θ_i is the inclination of the orbital plane to the reference $\{x, y\}$ plane which, in this case, is the SMBH's equator, and $u(t)$, which is the argument of latitude, represents the particle's orbital phase. By equating both expressions, one has $\cos \theta(t) = \sin \theta_i \sin u(t)$. The turning points are intended to be those where $|z_P| = |z_P|^{\max}$: the corresponding colatitudes occur at θ_\star and $\pi - \theta_\star$. Thus, the angle of the first turning point is $\theta_\star = \arccos(\sin \theta_i)$.

From Figure 2, it turns out that there are much more allowed regions for prograde orbits than for retrograde ones. In the first case, the effective radius may be as large as $50 r_{\text{ISCO}}^+$, while it can not be larger than $5 r_{\text{ISCO}}^-$ for the retrograde case. For the latter case, there are only about five allowed regions allowed corresponding to well detached multiples of r_{ISCO}^- . Instead, the permitted domains are much more numerous for the prograde case. Such a feature, arising phenomenologically from the aforementioned quite general assumptions, is in agreement with the conclusion drawn by Wang et al. (2025) with a more physical argument pertaining the measured disk's temperature and discussed in Section 4. For prograde orbits, the largest radii correspond to the highest possible values of the spin parameters. The corresponding part of the allowed region is, however, rather small, making such a scenario highly disfavored with respect to the one characterized by smaller radii and moderate BH's rotation rates. On the other hand, it turns out that the minimum allowed value of r_0 amounts to $1 r_{\text{ISCO}}^+$ just for two extremely narrow regions corresponding to $a_\bullet \simeq \pm 0.1$.

3.2 Narrowing the parameter space with the SMBH's mass

A sensible narrowing of the allowed region in the parameter space can be obtained by using the observational constrain on the SMBH's mass, which was determined by Wang et al. (2025) with two independent methods irrespectively of any dynamical model for the disk-jet coprecession: the single-epoch virial method and the M-sigma relation applied to spectral measurements taken before the TDE. Both resulted in consistent estimates yielding the value reported in Table 1. Furthermore, it contains also relevant parameters characterizing the space configuration of the system among which there is the angle θ_i entering $\hat{\mathbf{k}}_\bullet \cdot \hat{\mathbf{h}}$ in Equation (3). From the Supplementary Material provided by Wang et al. (2025), it seems that also such an angle, along with the other ones listed in Table 1 characterizing the orientation of the line of sight, was phenomenologically determined by fitting the 0.1 – 2 keV X-ray lightcurve over a time span three months long (August-October 2024) with a rigid precession model. Indeed, it appears that the hypothesis that the latter was explicitly due only to the LT effect was explicitly used later to constrain a_\bullet (see Eq. (S4) in Wang et al. (2025)).

Figure 3, produced by using Equation (3) calculated with the values of $\log(M_\bullet/M_\odot)$ and θ_i reported in Table 1, depicts the new permitted region in the three-dimensional parameter space $\{\log(M_\bullet/M_\odot), a_\bullet, r_0\}$.

It should be noted that, for $\theta_i = 14.5^\circ$, the first turning points' angle of the inclined orbit amounts to $\theta_\star = 75.5^\circ = 1.317$ rad. The left panel of Figure 5 of Kopáček and Karas (2024) clearly shows that the radii of the ISSOs are essentially identical to those of the ISCOs across the whole range for a_\bullet . Contrary to the prograde case, only three distinct allowed regions occur for a retrograde orbit corresponding to 2, 3 and $4 r_{\text{ISCO}}^-$. Thus, the prograde scenario is further strengthened with respect to the retrograde one. It appears evident how high values of the spin parameter are quite unlikely, being admitted only for a quite restricted allowed sub-domain of the overall permitted domain. The largest possible value for r_0 , corresponding to $a_\bullet = 1$, is $40 r_{\text{ISCO}}^+$. Interestingly, it can be shown that, according to Equation (23), the tidal disruption radius of a sun-like star ranges from about 7.5 to $35 R_g$ if it is calculated with the values

⁴In celestial mechanics, it is customarily denoted by I (Murray and Dermott, 1999). Here, for the sake of clarity, it is preferred to use the same symbol θ_i adopted for it by Wang et al. (2025).

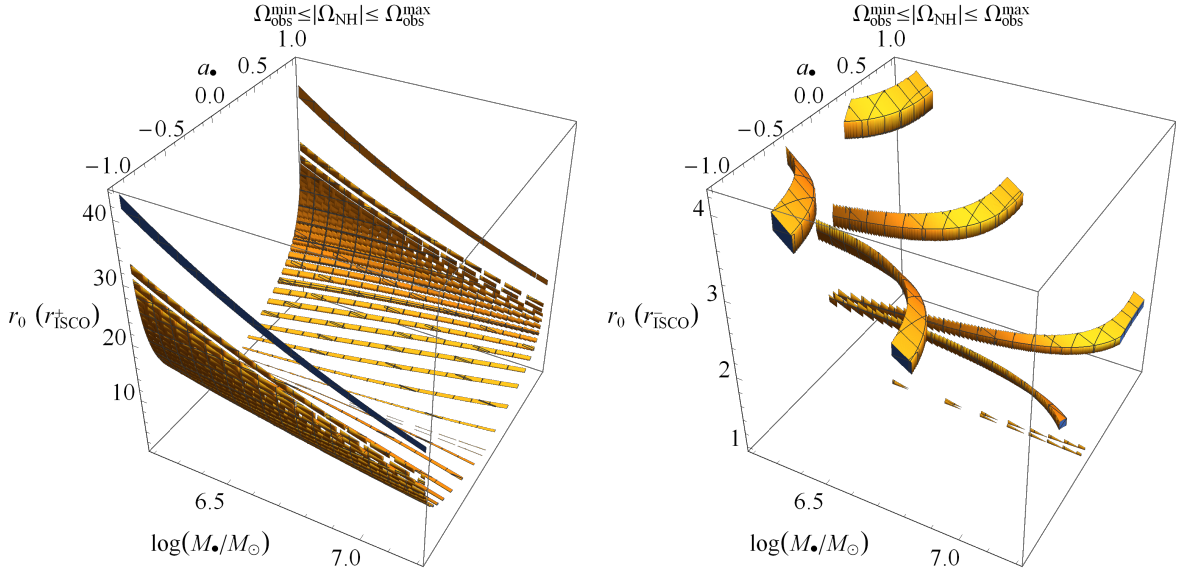


Figure 3: Permitted regions in the three-dimensional parameter space $\{\log(M_*/M_\odot), a_*, r_0\}$ obtained by imposing the conditions that the absolute value of the NH precessional frequency of Equation (3), calculated with Equations (7)–(8), lies within the experimental range of Equation (19) for the observed disk-jet coprecessional one, and that the radius r_0 of the effective test particle orbit is larger than that of the prograde (r_{ISCO}^+ , left panel) and retrograde (r_{ISCO}^- , right panel) equatorial ISCOs. The range of variation for $\log(M_*/M_\odot)$ and the best estimate for the colatitude θ_i of the orbital angular momentum were taken from Table 1, while a_* is allowed to vary within its full range $-1 \leq a_* \leq 1$.

of the Sun’s mass and radius and the experimental range of values for M_* listed in Table 1, amounting to $16.1 R_g$ for $\log(M_*/M_\odot) = 6.7$. In Wang et al. (2025), the external radius of the physical disk was assumed to be twice the tidal disruption radius.

3.3 Reducing the dimensionality of the parameter space by fixing the orbital radius

In fact, by fixing the effective radius r_0 to some value, one is left with just two independent variables: $\log(M_*/M_\odot)$ and a_* . To this aim, in the following, the reasonable, although bold assumption that

$$r_0 = r_t \quad (24)$$

will be made.

Figure 4 shows the allowed regions in the two-dimensional parameter space $\{\log(M_*/M_\odot), a_*\}$. It was obtained by using the values of the Sun’s mass and radius in Equation (23). Furthermore, it displays both the pure LT effect and the full NH bounds including also the impact of the SMBH’s quadrupole Q_2 , calculated with the value of θ_i reported in Table 1, in addition to the LT one. The resulting difference in the allowed ranges for a_* with and without Q_2 is of the order of about 0.01. It can be remarked that $r_t = 16.1 R_g$ is well larger than the maximum values of both the prograde and retrograde ISCOs’ radii.

Now, the overall allowed range of values for the SMBH’s spin parameter is

$$0.06 \leq a_* \leq 0.7, \quad (25)$$

where the width of the permitted intervals of a_* for given values of $\log(M_*/M_\odot)$ ranges from about 0.01 for $\log(M_*/M_\odot) \approx 7.2$ to at most 0.1 for $\log(M_*/M_\odot) \approx 6.2$. Furthermore, values of the spin parameter

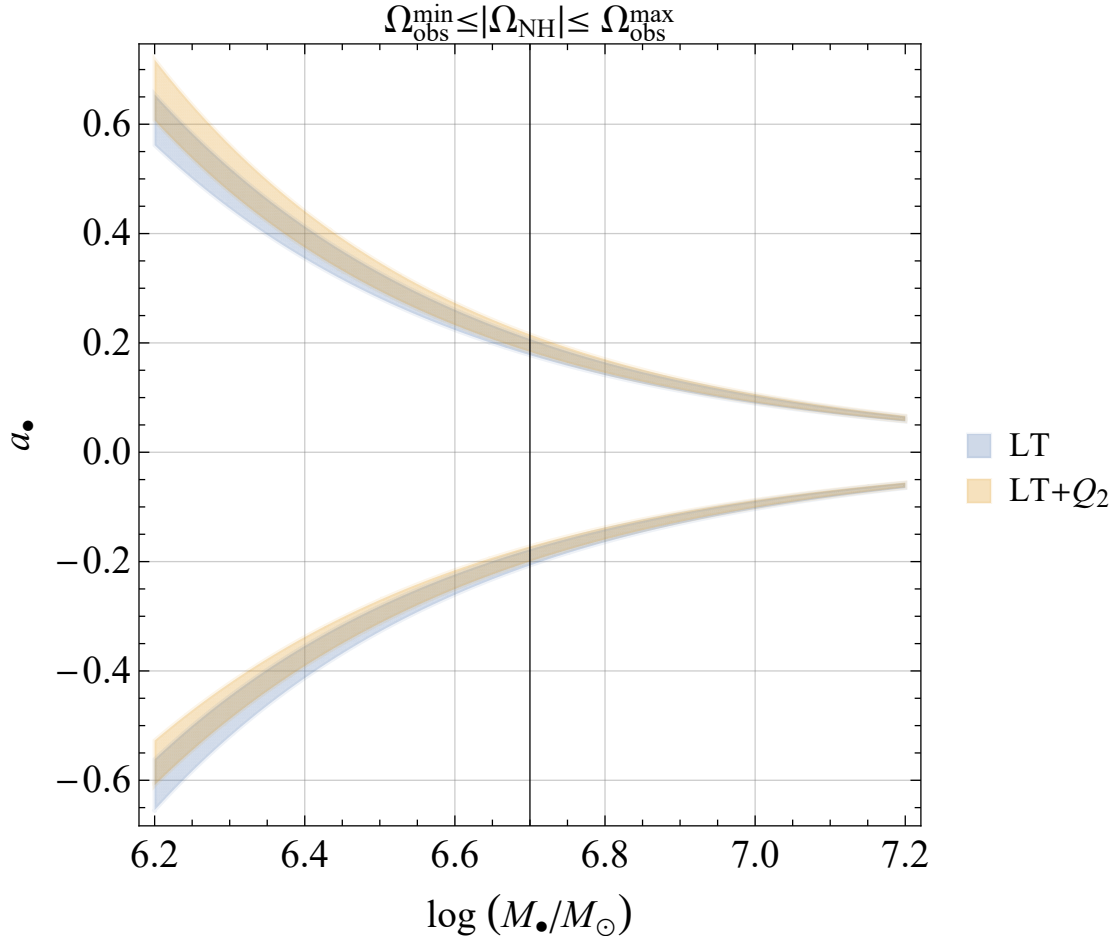


Figure 4: Permitted regions in the two-dimensional parameter space $\{\log(M_\bullet/M_\odot), a_\bullet\}$ obtained by imposing the condition that the absolute value of the NH precessional frequency of Equation (3), calculated with Equations (7)–(8), lies within the experimental range of Equation (19) for the observed disk-jet coprecessional one. The radius r_0 of the effective test particle orbit is set equal to the tidal disruption radius of Equation (23). The range of variation for $\log(M_\bullet/M_\odot)$ and the best estimate of the colatitude θ_i of the orbital angular momentum were taken from Table 1, while a_\bullet is allowed to vary within its full range $-1 \leq a_\bullet \leq 1$.

larger than ≈ 0.5 look disfavored since they correspond to a very narrow range of observationally admitted values for the SMBH’s mass. Instead, 82% of the entire allowed region of Figure 4 corresponds to $a_\bullet \lesssim 0.5$. In particular, $\log(M_\bullet/M_\odot) = 6.7$ gives

$$0.185 \lesssim a_\bullet \lesssim 0.215, \quad (26)$$

in substantial agreement with the range of positive values of Equation (29) reported in Wang et al. (2025) which, on the other hand, corresponds to about 47% of the overall allowed region in Figure 4. Furthermore, as explained in Section 4, it is unclear if Equation (29) can be really considered as a continuous range.

4 A discussion on the range for the BH's spin parameter by Wang et al. 2025

In their Section 6.1, Wang et al. (2025) adopted the following strategy to constrain the SMBH's spin parameter. As it will turn out, it relies upon model-dependent assumptions.

First, they considered only the LT effect as cause of the observed disk-jet coprecession, without including also the SMBH's quadrupole. Accordingly, they wrote down their Equation (S4) modelling the precession period for a physical thick disk of finite extension as⁵

$$T_{\text{prec}} = \frac{\pi G M_{\bullet} r_{\text{ms}}^3}{a_{\bullet} c^3} \frac{x_{\text{out}}^{5/2-\zeta} - 1}{1 - x_{\text{out}}^{-1/2-\zeta}} \frac{\zeta + 1/2}{5/2 - \zeta}. \quad (27)$$

In Equation (27), r_{ms} and x_{out} are dimensionless quantities denoting the radii of the ISCO and of the disk's outer boundary, respectively, in units of gravitational radii. To this aim, the double of the tidal disruption radius as given by Equation (23) was taken by Wang et al. (2025) for the disk's external radius; the internal radius was assumed by Wang et al. (2025) equal to ISCO's. Finally, ζ denotes⁶ a dimensionless power-law index for a disk's surface density profile for which the possible values $\zeta = 0, 3/5, 3/4$ were adopted by Wang et al. (2025).

Then, Wang et al. (2025) produced their Fig. 6 (A), obtained as follows. For each given value of the parameter ζ , they filled the space between the graphs of the absolute value of T_{prec} , given by Equation (27) and calculated with the minimum and the maximum determined values of $\log(M_{\bullet}/M_{\odot})$, as a function of a_{\bullet} getting three different gray-shaded regions. Importantly, they look different depending on whether a_{\bullet} is positive or negative. Finally, Wang et al. (2025) superimposed blue horizontal lines corresponding to the experimental range for T_{prec} which intersect the previously obtained domains in two narrow zones of different widths, highlighted by pink vertical bands. As a result, they claimed the following allowed continuous ranges for the SMBH's spin parameter

$$-0.46 \leq a_{\bullet} \leq -0.14, \quad (28)$$

$$0.11 \leq a_{\bullet} \leq 0.35. \quad (29)$$

The negative values were rejected by Wang et al. (2025) since, according to them, they would lead to a larger ISCO and, consequently, a larger inner disk radius, in contrast with the measured hot temperature for it.

Figure 5 displays the allowed regions in the $\{a_{\bullet}, T_{\text{prec}}\}$ plane reproduced in the present study according to the absolute value of Equation (27) for both prograde (left panel) and retrograde (right panel) ISCOs. It turns out that the prograde and retrograde panels of Figure 5 for $a_{\bullet} > 0$ and $a_{\bullet} < 0$, respectively, agree well with the half-planes $a_{\bullet} > 0$ and $a_{\bullet} < 0$ displayed in Fig. 6 (A) of Wang et al. (2025), respectively. At this point, a possible misunderstanding may arise about the statement by Wang et al. (2025) on the negative values of a_{\bullet} . In fact, it is not the negative sign of a_{\bullet} that makes the radius of the ISCO larger, but its retrograde character, as shown by Equations (14)–(17) and Figure 1. Thus, the physical reasons given by Wang et al. (2025) for seemingly rejecting the negative values of a_{\bullet} actually serve to exclude the retrograde ISCO, of whose picture they decided to show in Fig. 6 (A) only the part with $a_{\bullet} < 0$. Thus, the bound of Equation (28) is somehow misleading since it refers just to retrograde

⁵In the original version of the Supplementary Materials of Wang et al. (2025), a typo occurred in Equation (S4) which displayed the reciprocal of the two multiplicative factors of Equation (27) containing x_{out} and ζ .

⁶Here, the symbol ζ is adopted for it instead of p used in Wang et al. (2025) to avoid confusions with the semilatus rectum of the test particle's orbit.

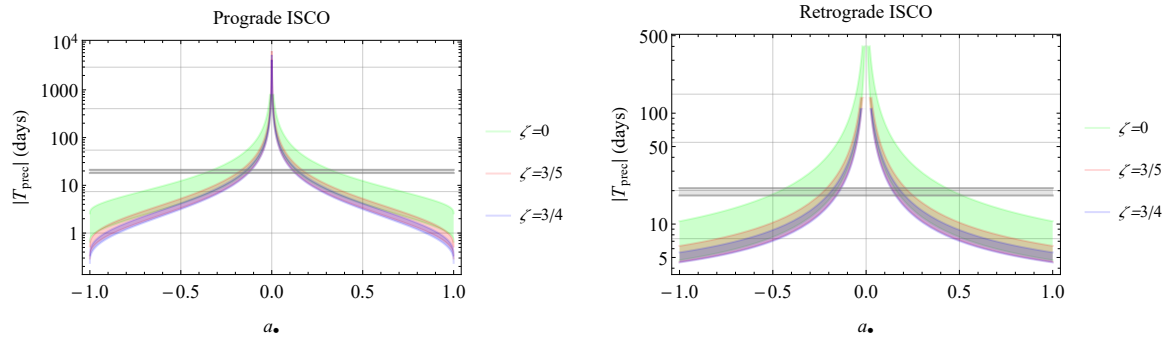


Figure 5: Allowed regions in the $\{a_\bullet, T_{\text{prec}}\}$ plane obtained by plotting the absolute value of Equation (27) versus a_\bullet for $\zeta = 0, 3/5, 3/4$ (Wang et al., 2025). Each shaded region is delimited by the log-linear plots obtained with the maximum and minimum values of $\log(M_\bullet/M_\odot)$, as per Table 1. Left panel: prograde ISCO. Right panel: retrograde ISCO.

ISCOs, which are ruled out. Given that only prograde ISCOs are likely permitted, Equation (28) should be replaced by the specular interval of Equation (29), namely $-0.35 \leq a_\bullet \leq -0.11$.

The values $\zeta = 0, 3/5, 3/4$ were not chosen by Wang et al. (2025) for any particular reason, as they are simply figures widely used in the literature. It must be remarked that the density profile of accretion disks is, actually, highly uncertain (Lu, 2022).

An equivalent approach to the one just followed, conveying the same amount of information and corresponding to the one adopted in Section 3, would consist in plotting the permitted domains in the parameter space $\{\log(M_\bullet/M_\odot), a_\bullet\}$ for each value of ζ by imposing that Equation (27) lies within the experimental range for T_{prec} as reported in Table 1. Figure 6, implementing it by assuming $|T_{\text{prec}}|$, shows

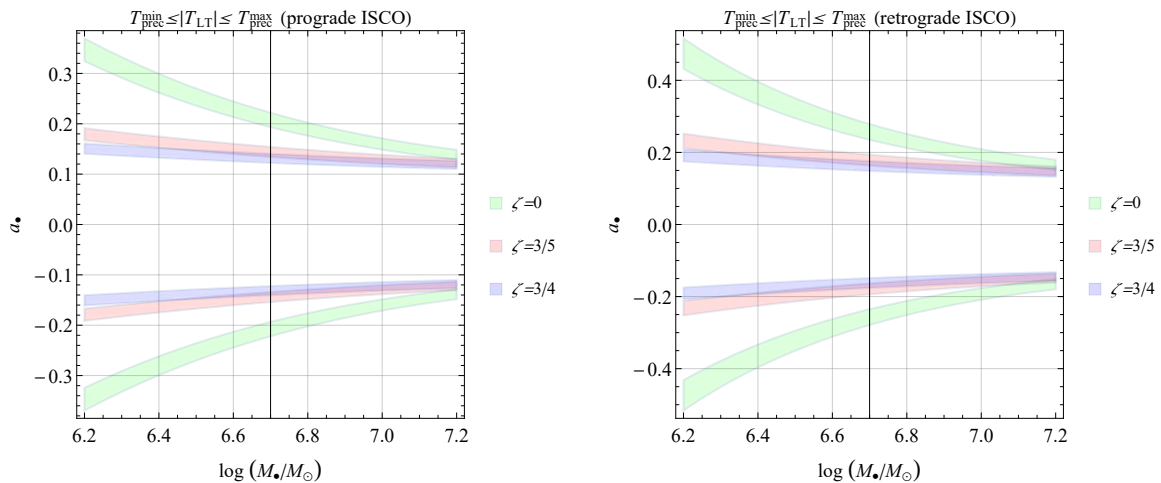


Figure 6: Allowed regions in the $\{\log(M_\bullet/M_\odot), a_\bullet\}$ plane obtained for $\zeta = 0, 3/5, 3/4$ (Wang et al., 2025) by imposing that the theoretical model of the absolute value of the period of the disk-jet coprocessions given by Equation (27) must lie within the experimental range of it as per Table 1. Left panel: prograde ISCO. Right panel: retrograde ISCO.

that some interpretational issues may arise for the bound of Equation (29). Indeed, both the panels of Figure 6 seem to suggest that it should not be considered as a continuous range, being, instead, replaced by up to three distinct smaller subranges, one for each value of ζ . It should be noted that only for the

retrograde ISCO there is a very small domain centered around about $\log(M_{\bullet}/M_{\odot}) \simeq 7.15 - 7.2$, $a_{\bullet} \simeq 0.1 - 0.13$ where all three regions overlap.

5 Summary and conclusions

A simple 1pN analytical model of the LT precession of the orbital angular momentum of a fictitious test particle moving along an effective circular orbit around a rotating material object is able to explain the main features of the recently observed disk-jet coprecession in the TDE associated with the optical transient AT2020afhd driven by the spinning SMBH of almost ten million solar masses in the core of the galaxy LEDA 145386.

A preliminary analysis based on quite general assumptions on TDEs shows that the allowed regions in the three-dimensional parameter space spanned by the SMBH's mass, its dimensionless spin parameter and the effective orbital radius, are much more numerous for prograde than for retrograde ISCOs, thus disfavoring the latter ones. Such permitted domains are obtained by only imposing the condition that the precession frequency analytically calculated with the aforementioned simple LT model lies within the experimental range for the measured rate of the disk-jet coprecession.

By using the measured interval of values of the SMBH's mass and setting the effective orbital radius equal to the tidal disruption one, narrower permitted domains in the two-dimensional mass-spin parameter space are obtained. While they are symmetric for negative and positive values of the spin parameter if only the LT effect is considered, the introduction of the further precession due to SMBH's quadrupole mass moment breaks this degeneracy. It turns out that, while the permitted range for the spin parameter extends from 0.06 up to 0.7, values larger than about 0.5 are disfavored since they correspond to less than 20% of the overall allowed domain. By adopting the best estimate for the SMBH's mass, the spin parameter is constrained within 0.185 – 0.215, in agreement with the recently published bounds.

It is explicitly demonstrated that both the LT and quadrupole formulas used here, based on precessional models about a spinning material body acting as primary, coincide with those obtainable from the expansion to the 1pN order of the geodesic equations of motion of a test particle in the Kerr metric describing the exterior spacetime of a rotating BH in general relativity.

The same strategy applied to the LT-only precession model used in the literature, which envisages an extended accretion disk of finite size endowed with a mass density profile parameterized in terms of a power-law index, yields to corresponding distinct allowed regions for different values of the latter which essentially do not overlap; they are overall comprised within the spin parameter's interval 0.11 – 0.35.

The approach presented here, successfully used in previous papers also for the measured precession of the jet emanating from the surrounding of the SMBH M87*, can be extended to precessional effects in other analogous scenarios allowing to predict their main features.

Data availability

No new data were generated or analysed in support of this research.

Conflict of interest statement

I declare no conflicts of interest.

Funding

This research received no external funding.

Acknowledgements

I thank Yanan Wang, Wei-Hua Lei, Weikang Lin and Yuzhu Cui for constructive discussions on a number of topics.

References

- R. M. Ali. Fluid sources for the Kerr metric. *Nuovo Cim. B*, 116:1009, 2001.
- M. Azreg-Ainou. From static to rotating to conformal static solutions: rotating imperfect fluid wormholes with(out) electric or magnetic field. *Eur. Phys. J. C*, 74:2865, 2014. doi: 10.1140/epjc/s10052-014-2865-8.
- J. M. Bardeen. Kerr Metric Black Holes. *Nature*, 226(5240):64–65, 1970. doi: 10.1038/226064a0.
- J. M. Bardeen, W. H. Press, and S. A. Teukolsky. Rotating Black Holes: Locally Nonrotating Frames, Energy Extraction, and Scalar Synchrotron Radiation. *Astrophys. J.*, 178:347–370, 1972. doi: 10.1086/151796.
- B. M. Barker and R. F. Oconnell. Effect of the rotation of the central body on the orbit of a satellite. *Phys. Rev. D*, 10:1340–1342, 1974. doi: 10.1103/PhysRevD.10.1340.
- R. H. Boyer and R. W. Lindquist. Maximal Analytic Extension of the Kerr Metric. *J. Math. Phys.*, 8: 265–281, 1967. doi: 10.1063/1.1705193.
- M. Calvani, F. de Felice, B. Muchotrzeb, and F. Salmistraro. Time machine and geodesic motion in Kerr metric. *Gen. Relativ. Gravit.*, 9:155–163, 1978. doi: 10.1007/BF00760150.
- J. K. Cannizzo, H. M. Lee, and J. Goodman. The Disk Accretion of a Tidally Disrupted Star onto a Massive Black Hole. *Astrophys. J.*, 351:38, 1990. doi: 10.1086/168442.
- B. Carter. Axisymmetric Black Hole Has Only Two Degrees of Freedom. *Phys. Rev. Lett.*, 26:331–333, 1971. doi: 10.1103/PhysRevLett.26.331.
- K. Chatterjee, Z. Younsi, M. Liska, A. Tchekhovskoy, S. B. Markoff, D. Yoon, D. van Eijnatten, C. Hesp, A. Ingram, and M. B. M. van der Klis. Observational signatures of disc and jet misalignment in images of accreting black holes. *Mon. Not. Roy. Astron. Soc.*, 499:362–378, 2020. doi: 10.1093/mnras/staa2718.
- Y.-C. Chou. An Interior Solution for the Kerr Metric: A Novel Approach. *Universe*, 11:23, Jan 2025. doi: 10.3390/universe11010023.
- J. M. Cohen. Note on the Kerr Metric and Rotating Masses. *J. Math. Phys.*, 8:1477–1478, 1967. doi: 10.1063/1.1705382.
- Chiara Coviello and Ruth Gregory. On extremal black holes. *arXiv e-prints*, art. arXiv:2512.01898, December 2025. doi: 10.48550/arXiv.2512.01898.

- Y. Cui and W. Lin. Co-precession of a curved jet and compact accretion disk in M87. *Nature Astronomy*, 9:1218–1225, 2025. doi: 10.1038/s41550-025-02580-0.
- Y. Cui, K. Hada, T. Kawashima, M. Kino, W. Lin, Y. Mizuno, H. Ro, M. Honma, K. Yi, J. Yu, J. Park, W. Jiang, Z. Shen, E. Kravchenko, J.-C. Algaba, X. Cheng, I. Cho, G. Giovannini, M. Giroletti, T. Jung, R.-S. Lu, K. Niinuma, J. Oh, K. Ohsuga, S. Sawada-Satoh, B. W. Sohn, H. R. Takahashi, M. Takamura, F. Tazaki, S. Trippe, K. Wajima, K. Akiyama, T. An, K. Asada, S. Buttaccio, D.-Y. Byun, L. Cui, Y. Hagiwara, T. Hirota, J. Hodgson, N. Kawaguchi, J.-Y. Kim, S.-S. Lee, J. W. Lee, J. A. Lee, G. Maccaferri, A. Melis, A. Melnikov, C. Migoni, S.-J. Oh, K. Sugiyama, X. Wang, Y. Zhang, Z. Chen, J.-Y. Hwang, D.-K. Jung, H.-R. Kim, J.-S. Kim, H. Kobayashi, B. Li, G. Li, X. Li, Z. Liu, Q. Liu, X. Liu, C.-S. Oh, T. Oyama, D.-G. Roh, J. Wang, N. Wang, S. Wang, B. Xia, H. Yan, J.-H. Yeom, Y. Yonekura, J. Yuan, H. Zhang, R. Zhao, and W. Zhong. Precessing jet nozzle connecting to a spinning black hole in M87. *Nature*, 621:711–715, 2023. doi: 10.1038/s41586-023-06479-6.
- M. Dafermos. The stability problem for extremal black holes: The stability problem for extremal black holes. *Gen. Relativ. Gravit.*, 57:60, 2025. doi: 10.1007/s10714-025-03394-1.
- J.L. Dai, G. Lodato, and R. Cheng. The Physics of Accretion Discs, Winds and Jets in Tidal Disruption Events. *Space Sci. Rev.*, 217:12, 2021. doi: 10.1007/s11214-020-00747-x.
- F. De Colle and W. Lu. Jets from Tidal Disruption Events. *New Astron. Rev.*, 89:101538, 2020. doi: 10.1016/j.newar.2020.101538.
- F. de Felice and M. Calvani. Causality violation in the Kerr metric. *Gen. Relativ. Gravit.*, 10:335–342, 1979. doi: 10.1007/BF00759491.
- J. Dexter and P. C. Fragile. Observational Signatures of Tilted Black Hole Accretion Disks from Simulations. *Astrophys. J.*, 730:36, 2011. doi: 10.1088/0004-637X/730/1/36.
- S. P. Drake and R. Turolla. The application of the Newman - Janis algorithm in obtaining interior solutions of the Kerr metric. *Class. Quantum Gravit.*, 14:1883–1897, 1997. doi: 10.1088/0264-9381/14/7/021.
- C. R. Evans and C. S. Kochanek. The Tidal Disruption of a Star by a Massive Black Hole. *Astrophys. J. Lett.*, 346:L13, 1989. doi: 10.1086/185567.
- L. Foschini. The physics of relativistic jets. *Front. Astron. Space Sci.*, 8:234, 2022. doi: 10.3389/fspas.2021.794891.
- L. Foschini, B. Dalla Barba, M. Tornikoski, H. Andernach, P. Marziani, A. P. Marscher, S. G. Jorstad, E. Järvelä, S. Antón, and E. Dalla Bontà. The Power of Relativistic Jets: A Comparative Study. *Universe*, 10(4):156, 2024. doi: 10.3390/universe10040156.
- P. C. Fragile, O. M. Blaes, P. Anninos, and J. D. Salmonson. Global General Relativistic Magnetohydrodynamic Simulation of a Tilted Black Hole Accretion Disk. *Astrophys. J.*, 668:417–429, 2007. doi: 10.1086/521092.
- A. Franchini, G. Lodato, and S. Facchini. Lense–Thirring precession around supermassive black holes during tidal disruption events. *Mon. Not. Roy. Astron. Soc.*, 455:1946–1956, 2016. doi: 10.1093/mnras/stv2417.

- K. Furusawa, H. Tashiro, S. Yokoyama, and K. Ichiki. Probing the Mass Relation between Supermassive Black Holes and Dark Matter Halos at High Redshifts by Gravitational Wave Experiments. *Astrophys. J.*, 959:117, 2023. doi: 10.3847/1538-4357/ad088f.
- R. Geroch. Multipole Moments. II. Curved Space. *J. Math. Phys.*, 11:2580–2588, 1970. doi: 10.1063/1.1665427.
- Y. Gürsel. Multipole moments for stationary systems: The equivalence of the Geroch-Hansen formulation and the Thorne formulation. *Gen. Relativ. Gravit.*, 15:737–754, 1983. doi: 10.1007/BF01031881.
- S. Haggag. A fluid source for the Kerr metric. *Nuovo Cim. B*, 105:365, 1990. doi: 10.1007/BF02728818.
- S. Haggag and J. Marek. A nearly-perfect-fluid source for the Kerr metric. *Nuovo Cim. B*, 62:273–282, 1981. doi: 10.1007/BF02721277.
- R. O. Hansen. Multipole moments of stationary space–times. *J. Math. Phys.*, 15:46–52, 1974. doi: 10.1063/1.1666501.
- K. Hayasaki, N. Stone, and A. Loeb. Circularization of tidally disrupted stars around spinning supermassive black holes. *Mon. Not. Roy. Astron. Soc.*, 461:3760–3780, 2016. doi: 10.1093/mnras/stw1387.
- W. C. Hernandez. Material Sources for the Kerr Metric. *Phys. Rev.*, 159:1070–1072, 1967. doi: 10.1103/PhysRev.159.1070.
- W. C. Hernandez. Kerr Metric, Rotating Sources, and Machian Effects. *Phys. Rev.*, 167:1180–1185, 1968. doi: 10.1103/PhysRev.167.1180.
- J. L. Hernandez-Pastora and L. Herrera. Interior solution for the Kerr metric. *Phys. Rev. D*, 95:024003, 2017. doi: 10.1103/PhysRevD.95.024003.
- L. Herrera and J. Jimenez. The complexification of a nonrotating sphere: an extension of the Newman-Janis algorithm. *J. Math. Phys.*, 23:2339–2345, 1982. doi: 10.1063/1.525325.
- J. G. Hills. Possible power source of Seyfert galaxies and QSOs. *Nature*, 254:295–298, 1975. doi: 10.1038/254295a0.
- L. Iorio. The no-hair theorems at work in M87*. *Mon. Not. Roy. Astron. Soc.*, 537:1470–1474, 2025a. doi: 10.1093/mnras/staf099.
- L. Iorio. Lense-Thirring effect at work in M87*. *Phys. Rev. D*, 111:044035, 2025b. doi: 10.1103/PhysRevD.111.044035.
- L. Iorio. Pyknons: A Suggestion for Rebranding Black Holes. *Universe*, 11:251, 2025c. doi: 10.3390/universe11080251.
- W. Israel. Event Horizons in Static Vacuum Space–Times. *Phys. Rev.*, 164:1776–1779, 1967. doi: 10.1103/PhysRev.164.1776.
- W. Israel. Source of the Kerr Metric. *Phys. Rev. D*, 2:641–646, 1970. doi: 10.1103/PhysRevD.2.641.
- R. T. Jantzen, P. Carini, and D. Bini. The many faces of gravitoelectromagnetism. *Ann. Phys. (N Y)*, 215:1–50, 1992. doi: 10.1016/0003-4916(92)90297-Y.
- R. P. Kerr. Gravitational Field of a Spinning Mass as an Example of Algebraically Special Metrics. *Phys. Rev. Lett.*, 11:237–238, 1963. doi: 10.1103/PhysRevLett.11.237.

- R. P. Kerr. Gravitational Collapse and Rotation. In I. Robinson, A. Schild, and E. L. Schucking, editors, *Quasi-Stellar Sources and Gravitational Collapse*, pages 99–102. University of Chicago Press, Chicago, 1965.
- O. Kopáček and V. Karas. On Innermost Stable Spherical Orbits near a Rotating Black Hole: A Numerical Study of the Particle Motion near the Plunging Region. *Astrophys. J.*, 966:226, 2024. doi: 10.3847/1538-4357/ad3932.
- A. Krasinski. Ellipsoidal space-times, sources for the Kerr metric. *Ann. Phys. (N Y)*, 112:22–40, 1978. doi: 10.1016/0003-4916(78)90079-9.
- E. Kyriakopoulos. Family of Rotating Anisotropic Fluid Solutions which Match to Kerr’s Solution. *Int. J. Mod. Phys. D*, 22:1350051, 2013. doi: 10.1142/S021827181350051X.
- K. Landsman. Singularities, Black Holes, and Cosmic Censorship: A Tribute to Roger Penrose. *Found. Phys.*, 51:42, 2021. doi: 10.1007/s10701-021-00432-1.
- M. Liska, C. Hesp, A. Tchekhovskoy, A. Ingram, M. van der Klis, and S Markoff. Formation of precessing jets by tilted black hole discs in 3D general relativistic MHD simulations. *Mon. Not. Roy. Astron. Soc.*, 474:L81–L85, 2018. doi: 10.1093/mnras/slx174.
- W. Lu. Accretion Disk Evolution in Tidal Disruption Events. In C. Bambi and A. Sanganello, editors, *Handbook of X-ray and Gamma-ray Astrophysics*, pages 1–24. Springer, Singapore, 2022. doi: 10.1007/978-981-16-4544-0_127-1.
- X. Ma, L. Tao, S.-N. Zhang, L. Zhang, Q.-C. Bu, M.-Y. Ge, Y.-P. Chen, J.-L. Qu, S. Zhang, F.-J. Lu, L.-M. Song, Y.-J. Yang, F. Yuan, C. Cai, X.-L. Cao, Z. Chang, G. Chen, L. Chen, T.-X. Chen, Y.-B. Chen, Y. Chen, W. Cui, W.-W. Cui, J.-K. Deng, Y.-W. Dong, Y.-Y. Du, M.-X. Fu, G.-H. Gao, H. Gao, M. Gao, Y.-D. Gu, J. Guan, C.-C. Guo, D.-W. Han, Y. Huang, J. Huo, L. Ji, S.-M. Jia, L.-H. Jiang, W.-C. Jiang, J. Jin, Y.-J. Jin, L.-D. Kong, B. Li, C.-K. Li, G. Li, M.-S. Li, T.-P. Li, W. Li, X. Li, X.-B. Li, X.-F. Li, Y.-G. Li, Z.-W. Li, X.-H. Liang, J.-Y. Liao, B.-S. Liu, C.-Z. Liu, G.-Q. Liu, H.-W. Liu, X.-J. Liu, Y.-N. Liu, B. Lu, X.-F. Lu, Q. Luo, T. Luo, B. Meng, Y. Nang, J.-Y. Nie, G. Ou, N. Sai, R.-C. Shang, X.-Y. Song, L. Sun, Y. Tan, Y.-L. Tuo, C. Wang, G.-F. Wang, J. Wang, L.-J. Wang, W.-S. Wang, Y.-S. Wang, X.-Y. Wen, B.-Y. Wu, B.-B. Wu, M. Wu, G.-C. Xiao, S. Xiao, F.-G. Xie, S.-L. Xiong, H. Xu, Y.-P. Xu, J.-W. Yang, S. Yang, Y.-J. Yang, Q.-B. Yi, Q.-Q. Yin, Y. You, A.-M. Zhang, C.-M. Zhang, F. Zhang, H.-M. Zhang, J. Zhang, T. Zhang, W.-C. Zhang, W. Zhang, W.-Z. Zhang, Y. Zhang, Y.-F. Zhang, Y.-J. Zhang, Y. Zhang, Z. Zhang, Z. Zhang, Z.-L. Zhang, H.-S. Zhao, X.-F. Zhao, S.-J. Zheng, D.-K. Zhou, J.-F. Zhou, Y.-X. Zhu, Y. Zhu, and R.-L. Zhuang. Discovery of oscillations above 200 keV in a black hole X-ray binary with Insight-HXMT. *Nature Astronomy*, 5: 94–102, 2021. doi: 10.1038/s41550-020-1192-2.
- B. Mashhoon. Gravitoelectromagnetism. In J. F. Pascual-Sánchez, L. Floría, A. San Miguel, and F. Vicente, editors, *Reference Frames and Gravitomagnetism*. World Scientific, 2001.
- B. Mashhoon. Gravitoelectromagnetism: A Brief Review. In L. Iorio, editor, *The Measurement of Gravitomagnetism: A Challenging Enterprise*, pages 29–39. Nova Science, 2007.
- J.C. McKinney, A. Tchekhovskoy, and R. D. Blandford. Alignment of Magnetized Accretion Disks and Relativistic Jets with Spinning Black Holes. *Science*, 339:49, 2013. doi: 10.1126/science.1230811.
- B. Mockler, E. Hammerstein, E.R. Coughlin, and M. Nicholl. Tidal Disruption Events. In I. Mandel, editor, *Encyclopedia of Astrophysics*, volume 3, pages 423–457. Elsevier, 2026. doi: 10.1016/B978-0-443-21439-4.00102-4.

- C. D. Murray and S. F. Dermott. *Solar System Dynamics*. Cambridge University Press, 1999. doi: 10.1017/CBO9781139174817.
- Y. C. Ong. Space-time singularities and cosmic censorship conjecture: A Review with some thoughts. *Int. J. Mod. Phys. A*, 35:2030007, 2020. doi: 10.1142/S0217751X20300070.
- T. Papakostas. Rotating fluids in General Relativity. In Spiros Cotsakis and John Miritzis, editors, *J. Phys. Conf. Ser.*, volume 8 of *Journal of Physics Conference Series*, pages 13–22. IOP, 2005. doi: 10.1088/1742-6596/8/1/002.
- D. R. Pasham, M. Zajaček, C. J. Nixon, E. R. Coughlin, M. Śniegowska, A. Janiuk, B. Czerny, T. Wevers, M. Guolo, Y. Ajay, and M. Loewenstein. Lense-Thirring precession after a supermassive black hole disrupts a star. *Nature*, 630:325–328, 2024. doi: 10.1038/s41586-024-07433-w.
- R. Penrose. Gravitational Collapse and Space-Time Singularities. *Phys. Rev. Lett.*, 14:57–59, 1965. doi: 10.1103/PhysRevLett.14.57.
- R. Penrose. The Question of Cosmic Censorship. *J. Astrophys. Astron.*, 20:233–248, 1999. doi: 10.1007/BF02702355.
- R. Penrose. “Golden Oldie”: Gravitational Collapse: The Role of General Relativity. *Gen. Relativ. Gravit.*, 7:1141–1165, 2002. doi: 10.1023/A:1016578408204.
- E. S. Phinney. Manifestations of a Massive Black Hole in the Galactic Center. In M. Morris, editor, *The Center of the Galaxy*, volume 136 of *IAU Symposium*, page 543, 1989.
- M. J. Rees. Tidal disruption of stars by black holes of 10^6 - 10^8 solar masses in nearby galaxies. *Nature*, 333:523–528, 1988. doi: 10.1038/333523a0.
- D. C. Robinson. Uniqueness of the Kerr Black Hole. *Phys. Rev. Lett.*, 34:905–906, 1975. doi: 10.1103/PhysRevLett.34.905.
- R. Ruffini and J. A. Wheeler. Introducing the black hole. *Phys. Today*, 62:47–53, 2009. doi: 10.1063/1.3120896.
- M. L. Ruggiero and A. Tartaglia. Gravitomagnetic effects. *Nuovo Cim. B*, 117:743, 2002.
- C. J. Saxton, R. Soria, K. Wu, and N. P. M. Kuin. Long-term X-ray variability of Swift J1644+57. *Mon. Not. Roy. Astron. Soc.*, 422:1625–1639, 2012. doi: 10.1111/j.1365-2966.2012.20739.x.
- S. L. Shapiro and S. A. Teukolsky. *Black Holes, White Dwarfs and Neutron Stars: The Physics of Compact Objects*. Wiley, 1986.
- S. L. Shapiro and S. A. Teukolsky. Formation of naked singularities: The violation of cosmic censorship. *Phys. Rev. Lett.*, 66:994–997, 1991. doi: 10.1103/PhysRevLett.66.994.
- N. Stone and A. Loeb. Observing Lense-Thirring Precession in Tidal Disruption Flares. *Phys. Rev. Lett.*, 108:061302, 2012. doi: 10.1103/PhysRevLett.108.061302.
- L. E. Strubbe and E. Quataert. Optical flares from the tidal disruption of stars by massive black holes. *Mon. Not. Roy. Astron. Soc.*, 400:2070–2084, 2009. doi: 10.1111/j.1365-2966.2009.15599.x.
- S. A. Teukolsky. The Kerr metric. *Class. Quantum Gravit.*, 32:124006, 2015. doi: 10.1088/0264-9381/32/12/124006.

- K. S. Thorne. Multipole expansions of gravitational radiation. *Rev. Mod. Phys.*, 52:299–340, 1980. doi: 10.1103/RevModPhys.52.299.
- K. S. Thorne. Black Holes: The Membrane Viewpoint. In S. L. Shapiro, S. A. Teukolsky, and E. E. Salpeter, editors, *Highlights of Modern Astrophysics: Concepts and Controversies*, pages 103–161. Wiley, 1986.
- K. S. Thorne. Gravitomagnetism, jets in quasars, and the Stanford Gyroscope Experiment. In J. D. Fairbank, Jr. Deaver, B. S., C. W. F. Everitt, and P. F. Michelson, editors, *Near Zero: New Frontiers of Physics*, pages 573–586. Freeman, 1988.
- K. S. Thorne, D. A. MacDonald, and R. H. Price, editors. *Black Holes: The Membrane Paradigm*. Yale University Press, 1986.
- P. Tian, P. Zhang, W. Wang, P. Wang, X. Sun, J. Liu, B. Zhang, Z. Dai, F. Yuan, S. Zhang, Q. Liu, P. Jiang, X. Wu, Z. Zheng, J. Chen, D. Li, Z. Zhu, Z. Pan, H. Gan, X. Chen, and N. Sai. Subsecond periodic radio oscillations in a microquasar. *Nature*, 621:271–275, 2023. doi: 10.1038/s41586-023-06336-6.
- A. Ulmer. Flares from the Tidal Disruption of Stars by Massive Black Holes. *Astrophys. J.*, 514: 180–187, 1999. doi: 10.1086/306909.
- S. Viaggiu. Interior Kerr Solutions with the Newman-Janis Algorithm Starting with Static Physically Reasonable Space-Times. *Int. J. Mod. Phys. D*, 15:1441–1453, 2006. doi: 10.1142/S0218271806009169.
- S. Viaggiu. Generating Anisotropic Fluids from Vacuum Ernst Equations. *Int. J. Mod. Phys. D*, 19: 1783–1795, 2010. doi: 10.1142/S0218271810018025.
- M. Visser. The Kerr spacetime: a brief introduction. In D. L. Wiltshire, M. Visser, and S. M. Scott, editors, *The Kerr Spacetime. Rotating Black Holes in General Relativity*, pages 3–37. Cambridge University Press, Cambridge, 2009.
- H. D. Wahlquist. Interior Solution for a Finite Rotating Body of Perfect Fluid. *Phys. Rev.*, 172:1291–1296, 1968. doi: 10.1103/PhysRev.172.1291.
- Y. Wang, Z. Lin, L. Wu, W. Lei, S. Wei, S.-N. Zhang, L. Ji, S. del Palacio, R. D. Baldi, Y. Huang, J. Liu, B. Zhang, A. Yang, R. Chen, Y. Zhang, A. Wang, L. Yang, P. Charalampopoulos, D. R. A. Williams-Baldwin, Z.-H. Yao, F.-G. Xie, D. Bu, H. Feng, X. Cao, H. Wu, W. Li, E. Qiao, G. Leloudas, J.P. Anderson, X. Shu, D.R. Pasham, H. Zou, M. Nicholl, T. Wevers, T. E. Muller-Bravo, J. Wang, J. Wei, Y.-L. Qiu, W. Guo, C. P. Gutierrez, M. Gromadzki, C. Inerra, L. Makrygianni, F. Onori, T. Petrushevska, D. Altamirano, L. Galbany, M. Perez-Torres, and T.-W. Chen. Detection of disk-jet co-precession in a tidal disruption event. *Science*, 11:eady9068, 2025. doi: 10.1126/sciadv.ady9068.
- C. M. Will. Inaugural Article: On the unreasonable effectiveness of the post-Newtonian approximation in gravitational physics. *Proc. Natl. Acad. Sci.*, 108:5938–5945, 2011. doi: 10.1073/pnas.1103127108.